applied optics

Micro-capillary-based self-referencing surface plasmon resonance biosensor for determination of transferrin

Shimeng Chen, Yun Liu, Zigeng Liu, Shuwen Chu, and Wei Peng*

School of Physics and Optoelectronic Technology, Dalian University of Technology, 2 Linggong Rd., Ganjingzi District, Dalian 116024, China
**Corresponding author: wpeng@dlut.edu.cn*

Received 19 May 2016; revised 18 September 2016; accepted 20 September 2016; posted 20 September 2016 (Doc. ID 265489); published 20 October 2016

A novel self-referencing surface plasmon resonance (SPR) biosensor for detection of transferrin is demonstrated using a micro-capillary as the sensing element. The biosensor employs the SPR mode as a measuring signal and the Fabry–Perot (FP) mode as a referencing signal. The SPR mode is generated in the gold film that is coated on the outside of the capillary; instead, the FP mode is excited in the capillary, which is filled with de-ionized water. The FP mode is sensitive to temperature and insensitive to refractive index, which can be used as a referencing signal to compensate the effects caused by the temperature fluctuation. The sensor provides a high sensitivity of 1783.943 nm/RIU (refractive index unit) and a resolution of about 7.287×10^{-5} RIU. The self-referencing biosensor was applied to measurement of transferrin protein. It can monitor the interaction of transferrin protein with anti-transferrin in real time (0–5.228 μM). The simple and low-cost SPR sensor can be used for highly sensitive self-referencing biosensing for further investigations.

OCIS codes: (240.6680) Surface plasmons; (060.2370) Fiber optics sensors; (280.1415) Biological sensing and sensors.

http://dx.doi.org/10.1364/AO.55.008571

1. INTRODUCTION

Surface plasmon resonance (SPR) is an ideal technology for label-free detection and biomolecular interaction analysis [1–4]. Due to the small size, high sensitivity, fast response, and real-time detection, the fiber-optic SPR sensors have been widely used in biochemical and biological applications [5–7]. Different fiber-optic SPR sensors have been demonstrated, such as SPR sensors based on tapered fiber [8], D-type fiber [9], photonic crystal fiber [10], and light-guiding flexible fused-silica capillary tubing [11]. Due to their unique advantages of high sensitivity, miniaturization, remote sensing, unlabeling and *in situ* detection, the fiber-optic SPR sensors are suitable for the detection of water quality, chemicals, and biomolecules. For *in situ* applications, environmental conditions, especially temperature fluctuations, greatly influence the performance of fiber-optic SPR sensors. Thus, temperature compensation capability of fiber-optic SPR sensors is very important. It has been reported that many SPR sensors have compensating functions [12–17]. Shao *et al.* [12] designed a SPR sensor based on tilted fiber Bragg grating (TFBG), providing a calibrated value for residual temperature dependence of the SPR shift to compensate the thermo-optical effects of the sensor itself and the temperature effects of the samples, without influence from the outer medium refractive index. However, the production process of TFBG is very complicated and expensive. Zhang *et al.* [13] reported a temperature-compensating SPR that provided two SPR resonance wavelengths using different coatings. By choosing a reference material with a very large thermo-optic coefficient, the sensor demonstrated an SPR optical fiber sensor that can correct the effects of temperature variation in the testing medium by itself. Nonetheless, due to the uncontrollable thickness of the reference material, temperature compensation capability could be easily influenced. Naimushin *et al.* [14] presented a dual-channel SPR sensor, which is similar to a Spreeta TM instrument. This dual-channel method can completely compensate non-specific binding and temperature effects. But this sensor is not suitable for chemical and biomedical sensing applications because of its large volume. Slavík *et al.* [15] proposed a novel fiber-optic biosensor that exploits simultaneous excitation of symmetric and anti-symmetric bound surface plasmons in a single sensing spot. It allows compensation of cross-sensitivity to background refractive index change. Teflon AF was used as the buffer layer in combination with gold, so the manufacture cost of this biosensor was increased by the complicated manufacturing process. Hasting *et al.* [16] reported a SPR sensor supporting long- and short-range surface-plasmon modes, which also use high molecular polymer (Teflon AF) as the buffer layer. Bahrami *et al.* [17]

demonstrated a plasmon waveguide resonance (PWR) sensor. The self-referencing sensor was able to support two different polarizations, TM and TE. The TM mode is highly sensitive to the refractive index change in bulk solution while the TE mode was more sensitive to the thickness change of the attached streptavidin layer. The PWR sensor provided the ability to decouple surface and bulk effects via multimode spectroscopy. These sensors have a high cost and complicated manufacturing process.

Comparing to these sensors with complex structure and high price, the self-referencing SPR biosensor we demonstrated in this paper has many advantages, such as miniaturization, simple structure, and cost-effectiveness. Instead of fiber, the key sensing area of our biosensor is the micro-capillary. As a novel sensing element, the capillary was used in the fields of temperature sensing [18], biological detection [19], and SPR sensing [11,20]. Unlike other reported self-referencing sensors, the capillary as the only sensing element in our biosensor is spliced between two multimode fibers (MMFs). The SPR effect occurs in the tubing wall used for the measuring signal, and the Fabry–Perot (FP) mode induced by the de-ionized water filling capillary is used as the referencing signal. Benefiting from the temperature-sensitive and refractive index-insensitive FP element, the SPR biosensor effectively eliminates the effects of external environmental temperature. The sensor was validated by a temperature testing system and was used to detect specific transferrin protein.

2. EXPERIMENTAL SETUP AND PRINCIPLES

The experimental setup is shown in Fig. 1(a). In this experiment, we used a tungsten-halogen lamp (HL-2000-FHSA, Ocean Optics) as the light source with wide spectra, which could vary continuously from 400 to 1000 nm. The spectrometer (USB4000, Ocean Optics) was used to detect the signals of transmission from the sensor. A laptop is connected with a spectrometer to record and process the experimental data.

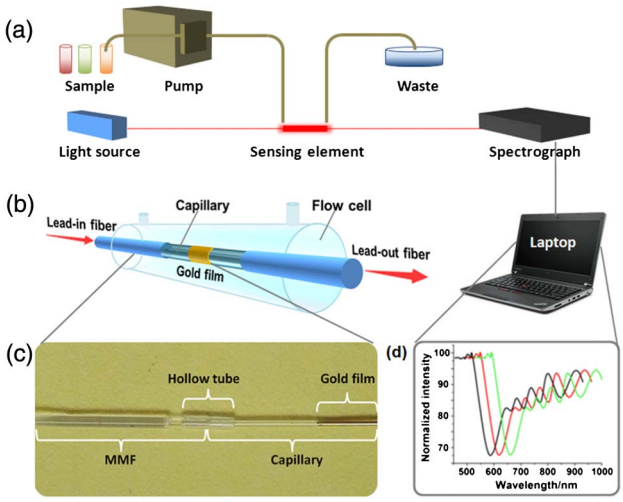

Fig. 1. Schematic diagram of the self-referencing SPR sensing system. (a) The experimental setup of the sensor; (b) the sensing element of the sensing system; (c) the photograph of the sensing element; (d) the transmission spectra.

As shown in Fig. 1(b), we chose the plastic optical fiber (HP 400/430-37/730EYOFC) as the lead-in and lead-out fibers, which were connected to the light source and the spectrograph via SMA 905 connectors. The sensing element is fabricated by a 20 mm long fused-silica capillary (TSP250/350, Polymicro Inc.) without a polyimide jacket and is coated with a gold film by a magnetron sputtering coater (K575XD, E.M. Technologies Ltd.). The length of the sensing region and the thickness of the gold film were 5 mm and 50 nm, respectively. The MMFs were spliced with a piece of capillary using a hollow tube and glue. The photograph of the sensing element is shown in Fig. 1(c). Using a home-made flow cell as the reaction tank, the sample was pumped with a peristaltic pump (BT-100 2J, Longer), and the SPR sensing system was monitored by the Labview software. In addition, light propagated in the tube wall and the capillary was filled with the de-ionized water. So the SPR mode and FP mode can occur at the same time. The transmission spectra with measuring and referencing signals are shown in Fig. 1(d). To eliminate the influence of the environmental temperature, instead of using a dual-channel sensor, we used a single sensing element in this device. Its unique advantages made the self-referencing SPR device simple without an additional channel, which was also convenient for the fabrication of the sensor.

Figure 2 shows the operating principles of this self-referencing fiber-optic SPR biosensor. We tested the characteristics of the sensing element under different experimental conditions, respectively. The experimental setup is shown in

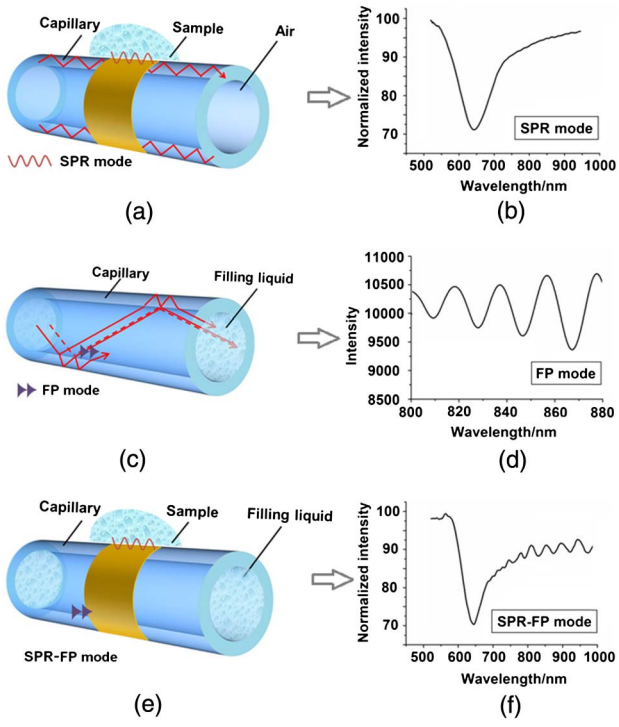

Fig. 2. Principles of the self-referencing fiber-optic SPR biosensor. (a) Schematic diagram of the SPR mode; (b) transmission spectra of the SPR mode; (c) schematic diagram of the FP mode; (d) transmission spectra of the FP mode; (e) schematic diagram of the SPR-FP mode; (f) transmission spectra of the SPR-FP mode.

Fig. 1(a) and the de-ionized water as the analyte was pumped into a flow cell in experiments. The path of the SPR mode is revealed in Fig. 2(a). Light propagated in the tubing wall and excited the SPR mode in the sensing region where the silica surface was coated with a 50 nm gold film. Unlike the capillary-based SPR sensor reported [11], this sensor we designed does not need the chemical etching technique. The transmission spectra of the SPR mode are shown in Fig. 2(b), from which we can find that the absorbance of the SPR resonance peak can reach 30%. Figure 2(c) shows the path of the FP mode. On the basis of the Fresnel's laws of reflection, we analyzed the behavior of the light sense. When the light reaches the inner wall of the capillary, some of the light is reflected by the inner wall and the remaining part is refracted. The refracted light enters in the tubing wall and is reflected by the outer wall of the capillary. The light reflected by the inner wall and outer wall propagates in the capillary and interferes with each other, which is similar to FP interference [20]. Reflectivity and refractivity are determined by the incident angle of light and the refractive index of the filling liquid. In order to investigate the influence of the filling liquid with different refractive indices, the capillary was filled with air, de-ionized water, and ethanol. As the refractive index of the filling liquid increased, the intensity of the light increased and the visibility of the fringe decreased. Because the capillary filled with the de-ionized water had good intensity and clear interference fringes, we chose the de-ionized water as the filling liquid. To validate the feasibility of the sensing element, we fabricated and tested several sensing elements with different lengths. Finally, 2 mm length was selected as the optimal length of the sensing region; the transmission spectrum of the FP mode is shown in Fig. 2(d). The sensing element can realize the dual-channel sensing with the capillary filled with the de-ionized water and coated with gold film. Figure 2(f) shows the transmission spectrum of the SPR-FP mode. It can be found that the SPR signal appears within the range of 600–700 nm and has a deep absorption. Then, the FP signal has a clear fringe within the range of 800–1000 nm and has little impact on the SPR signal. Thus, the cross talk between the measuring and referencing signals is almost negligible using simple the digital filter method. So the sensing element we designed can provide the sharp interference fringes and the stable SPR transmission spectra.

3. RESULTS AND DISCUSSION

We investigated the characteristics of the transmission spectra of the sensing element through temperature and refractive index tests. We chose the dip of the FP interference fringe in the 851.5 nm as the referencing signal. The sodium chloride solutions were prepared as calibration samples, whose refractive indices were calibrated with an Abbe refractometer (WAY-2S). At a constant temperature (20°C), the sodium chloride solutions with the refractive indices of 1.3314, 1.3402, 1.3489, 1.3574, and 1.3662 were delivered into a flow cell at a constant flow rate of 0.1 ml/min via a peristaltic pump. Figure 3 shows the refractive index response of the sensing element. The SPR transmission spectra are shown in Fig. 3(a). As the refractive indices of the samples increase, the SPR dip shifts to a longer wavelength. The calibration curve is obtained

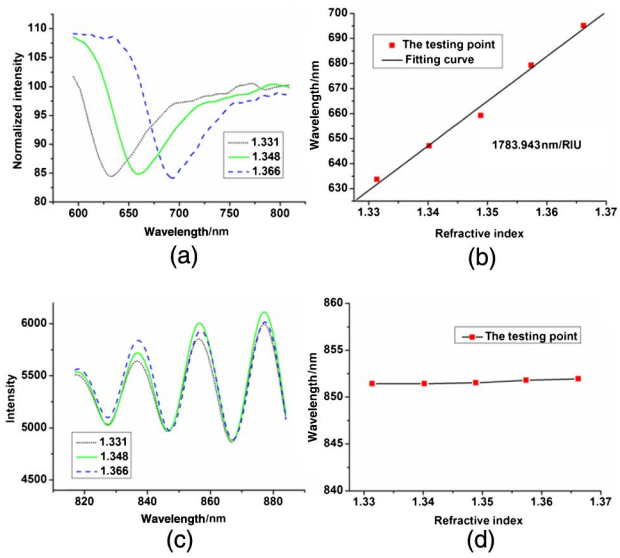

Fig. 3. Refractive index characteristics of the dual-mode sensing element. (a) and (b) Refractive index responses of the SPR mode; (c) and (d) refractive index responses of the FP mode.

using the least-square method. The system provided a refractive index sensitivity of 1783.943 nm/RIU [Fig. 3(b)] and a resolution of about 7.287×10^{-5} RIU within the range of 1.3314–1.3662, which includes the range for most common biofluids. The refractive index characteristic of the FP interference fringe is revealed in Figs. 3(c) and 3(d). As the refractive indices of the samples change, the total wavelength fluctuation of the FP interference fringe is less than 0.2 nm. The FP mode has little response, which means the FP mode is almost insensitive to the refractive index.

For the fiber-optic SPR sensor, temperature effect is a main disturbance factor for *in situ* measurement. This novel sensing element we designed can provide a temperature compensation for accurate measurement. To evaluate the compensating performance of the sensing element, we tested the temperature sensitivity of the sensor. The sensing element was heated in a water bath from 20°C to 60°C with 10°C steps. With the variation of temperature, both the SPR signal and FP signal had obvious wavelength shifts. Figure 4(a) shows the transmission spectra of the SPR mode. The wavelength of the SPR signal shifts to a shorter wavelength when the temperature increases. After least-squares fitting, the slope of the temperature response calibration curve is −0.316 nm/°C over a 40°C range. The transmission spectra of the FP interference fringe [Fig. 4(c)] have a similar linear response to temperature with the SPR mode. The temperature sensitivity of the FP mode is −0.148 nm/°C. Considering that the resolution of the spectrometer is 0.13 nm, the temperature resolutions of the measurement and reference channels are 0.411°C and 0.878°C, respectively. Based on the data, the FP mode can be used as the compensation signal for experimental measurement.

Because the FP mode is sensitive to temperature, but is insensitive to refractive index, it can be used as a referencing signal for temperature compensation. To verify the feasibility of the temperature compensation performance of this biosensor,

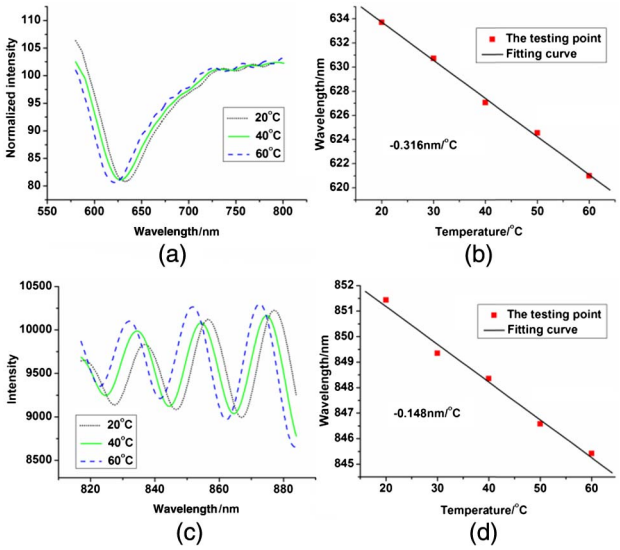

Fig. 4. Temperature characteristics of the dual-mode sensing element. (a) and (b) Temperature responses of the SPR mode; (c) and (d) temperature responses of the FP mode.

the temperature fluctuation experiment was performed. In this work, we employed a fiber Bragg grating (FBG) sensor as a temperature sensor to measure the temperature in a flow cell. The main advantages of the FBG are shorter response time, lower cost, high accuracy, and more convenient to use [21]. During the calibration, the FBG was heated in a water bath and was submitted to a temperature variation of 25°C to 75°C with 10°C steps. The temperature sensitivity is 9.12 pm/°C. The two-channel sensor and the FBG sensor were put in a flow cell simultaneously and the responses of the two sensors for 1400s were recorded under the irregular temperature change. Both channels reveal obvious wavelength shift. The temperature responses of the SPR mode and the FP mode are shown as the black line and green line in Fig. 5(a). The two signals reveal the similar trend of wavelength shift, which is consistent with the above result. Using the temperature sensitivities of the SPR mode and the FP mode, the temperature responses of the two channels can be calibrated. The calibration signal can be obtained [the red line in Fig. 5(b)] by subtracting two signals. Compared with the test temperature, the calibration curve is relatively stable and temperature effects are

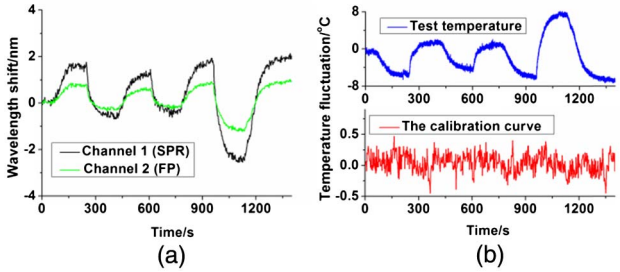

Fig. 5. Temperature-compensating characteristics. (a) The wavelength shifts of two channels under temperature fluctuation and (b) the test temperature curve and the calibration curve of two channels under temperature fluctuation.

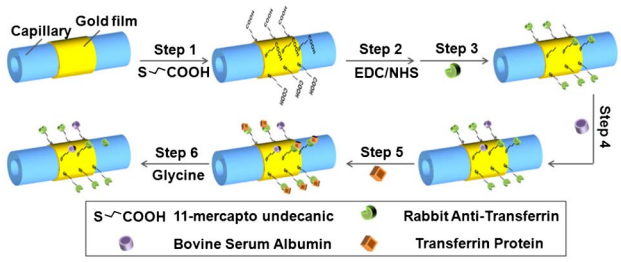

Fig. 6. Anti-transferrin immobilization protocol on the sensing surface.

basically eliminated. The average fluctuation margin of the temperature is below ±0.5°C.

In addition, to test the biosensing of the SPR biosensor, the functionalized SPR biosensor was tested for real-time detection of transferrin protein sample. The immobilization of anti-transferrin was performed, as depicted in Fig. 6. Before surface functionalization of the sensing probe, the sensing probe was ultrasonically cleaned with the de-ionized water, ethanol, dichloromethane, and ethanol. After a subsequent wash, the sensor was soaked in 1 mM 11-mercaptoundecanoic acid molecules in ethanol at a constant temperature (20°C) for 24 h to form an alkanethiol self-assembled monolayer on the gold film. Subsequently, the sensing surface was soaked in the ultrapure water of 0.5 M N-hydroxysuccinimide and 0.55 M 1-ethyl-3-(3-dimethylamino-propyl) carbodiimide hydrochloride at 4°C for 30 min to convert the carboxyl surface to activated ester. After being dried under nitrogen, the treated sensor was rinsed with 0.01 M phosphate-buffered saline (PBS, pH = 7.4), and then was immersed in 0.1 mg/ml anti-transferrin (0.1 mg/ml in PBS buffer) for 30 min. After rinsing in the PBS buffer, the sensor was immersed in 1 mg/ml bovine serum albumin at a constant temperature (20°C) for 15 min. The purpose of the last step is to deactivate the remaining activated esters and to prevent non-specific site binding. The sensing probe had been functionalized at this point. Then, the sensing probe was mounted onto a flow cell and connected with the light source and spectrometer for specific binding of transferrin protein.

During the testing, the SPR measuring and FP referencing signals were recorded at a constant temperature (20°C). Transferrin protein samples with different concentrations were prepared in the PBS buffer. A series of aqueous solutions (PBS buffer, transferrin protein sample, PBS buffer, glycine sample) were pumped into a flow cell at a constant flow rate of 0.5 mL/min. To start with, the PBS buffer was introduced to establish the baseline value. Figure 7(a) shows that the response of the SPR absorption dip has a redshift with the injection of the transferrin protein sample, which is consistent with the fact that anti-transferrin binds specifically to transferrin protein on the sensing surface. Then the PBS buffer was introduced, and the response has a slight decrease because of the PBS buffer flowing over the sensing surface to physically wash off the adsorbed transferrin protein molecules. Glycine (10 mM) was used to regenerate the functional surface of the sensing element.

In addition, each measurement at a given concentration was repeated thrice. We can find that the measurement results of wavelength responses had good repeatability. The standard

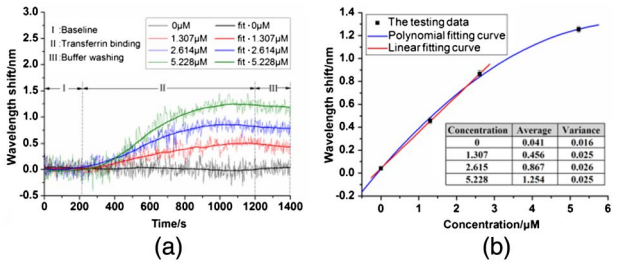

Concentration	Average	Variance
0	0.041	0.016
1.307	0.456	0.025
2.615	0.867	0.026
5.228	1.254	0.025

Fig. 7. Detection of specific binding between transferrin protein and anti-transferrin of the fiber-optic SPR biosensor. (a) Different responses for detection of specific binding with transferrin protein at the concentration of 0–5.228 μM (I: baseline; II: transferrin binding; III: buffer washing) and (b) the relationship between the measured wavelength shifts and the sample concentrations.

deviations of different concentrations were less than 0.026 [the inset in Fig. 7(b)]. The relationship between the wavelength shifts and the concentrations of transferrin protein were shown in Fig. 7(b). Through four rounds of transferrin protein detection at different concentrations (0, 1.307, 2.614, and 5.228 μM), the SPR responses became stronger as the transferrin protein concentration increased. It means more transferrin protein is specifically bound with anti-transferrin when the concentrations of transferrin protein increase. The wavelength response of the SPR biosensor appeared approximately at the low sample concentration. Then, the binding site approached saturation, and the growth rate was slowed with the increase of the concentrations of transferrin protein.

4. CONCLUSION

A novel micro-capillary-based self-referencing SPR biosensor has been demonstrated, with a high sensitivity of 1783.943 nm/RIU and a resolution of about 7.287×10^{-5} RIU. This biosensor employed the SPR mode and FP mode as the measuring and referencing signals, respectively. We analyzed the characteristics of both modes in the paper. The temperature responses of the measuring and referencing signals are −0.316 nm/°C and −0.148 nm/°C. Since the temperature sensitivity of the referencing signal has a magnitude equal to that of the measuring signal, the temperature correction is accurate and it is possible to correct any errors caused by changes in external environmental temperature in most of the biological and environmental sensing applications. The feasibility of the temperature compensating performance of this biosensor was verified in the temperature fluctuation experiment. Then, the self-referencing SPR biosensor was applied for the biosensing of transferrin protein with the immobilization of anti-transferrin on a gold film of the sensing element. The test results show that the SPR biosensor can detect the binding process with an approximate linear relative response within the analyte concentration range of 0–5.228 μM. This self-referencing SPR biosensor has the advantage of high sensitivity, favorable resolution, simple manufacturing process, reliable quality, and cost-effectiveness. This biosensor has a great potential for biological and biochemical applications and can be applied to real-time and on-site detection.

Funding. Ministry of Education of the People's Republic of China (MOE) (SRFDP-20120041110040); National Natural Science Foundation of China (NSFC) (61137005, 61520106013).

REFERENCES

1. T. M. Chinowsky, M. S. Grow, K. S. Johnston, K. Nelson, T. Edwards, E. Fu, and P. Yager, "Compact, high performance surface plasmon resonance imaging system," Biosens. Bioelectron. **22**, 2208–2215 (2007).
2. J. Homola, "Surface plasmon resonance sensors for detection of chemical and biological species," Chem. Rev. **108**, 462–493 (2008).
3. D. R. Shankaran, K. V. Gobi, and N. Miura, "Recent advancements in surface plasmon resonance immunosensors for detection of small molecules of biomedical, food and environmental interest," Sens. Actuators B **121**, 158–177 (2007).
4. Y. Liu, Q. Liu, S. M. Chen, F. Cheng, H. Q. Wang, and W. Peng, "Surface plasmon resonance biosensor based on smart phone platforms," Sci. Rep. **5**, 12864 (2015).
5. A. K. Sharma, R. Jha, and B. D. Gupta, "Fiber-optic sensors based on surface plasmon resonance: a comprehensive review," IEEE Sens. J. **7**, 1118–1129 (2007).
6. J. H. Ahn, T. Y. Seong, W. M. Kim, T. S. Lee, I. Kim, and K. S. Lee, "Fiber-optic waveguide coupled surface plasmon resonance sensor," Opt. Express **20**, 21729–21738 (2012).
7. S. K. Srivastava, R. Verma, and B. D. Gupta, "Surface plasmon resonance based fiber optic sensor for the detection of low water content in ethanol," Sens. Actuators B **153**, 194–198 (2011).
8. Y. C. Kim, W. Peng, S. Banerji, and K. S. Booksh, "Tapered fiber optic surface plasmon resonance sensor for analyses of vapor and liquid phases," Opt. Lett. **30**, 2218–2220 (2005).
9. M. H. Chiu, S. F. Wang, and R. S. Chang, "D-type fiber biosensor based on surface-plasmon resonance technology and heterodyne interferometry," Opt. Lett. **30**, 233–235 (2005).
10. J. N. Dash and R. Jha, "SPR biosensor based on polymer PCF coated with conducting metal oxide," IEEE Photon. Technol. Lett. **26**, 595–598 (2014).
11. X. X. Liu, Y. Liu, Q. Liu, X. T. Gao, and W. Peng, "Surface plasmon resonance biochemical sensor based on light guiding flexible fused silica capillary tubing," Opt. Commun. **356**, 212–217 (2015).
12. L. Y. Shao, Y. Shevchenko, and J. Albert, "Intrinsic temperature sensitivity of tilted fiber Bragg grating based surface plasmon resonance sensors," Opt. Express **18**, 11464–11471 (2010).
13. Z. Zhang, P. Zhao, F. Sun, G. Xiao, and Y. Wu, "Self-referencing in optical-fiber surface plasmon resonance sensors," IEEE Photon. Technol. Lett. **19**, 1958–1960 (2007).
14. N. Naimushin, S. D. Soelberg, D. U. Bartholomew, J. L. Elkind, and C. E. Furlong, "A portable surface plasmon resonance (SPR) sensor system with temperature regulation," Sens. Actuators B **96**, 253–260 (2003).
15. R. Slavík, J. Homola, and H. Vaisocherová, "Advanced biosensing using simultaneous excitation of short and long range surface plasmons," Meas. Sci. Technol. **17**, 932–938 (2003).
16. J. T. Hasting, P. D. Keathley, P. B. Kumaresh, Y. Wei, S. Law, and L. G. Bachas, "Optimal self-referenced sensing using long- and short-range surface plasmons," Opt. Express **15**, 17661–17672 (2007).
17. F. Bahrami, M. Maisonneuve, M. Meunier, J. S. Aitchison, and M. Mojahedi, "Self-referenced spectroscopy using plasmon waveguide resonance biosensors," Biomed. Opt. Express **5**, 2481–2487 (2015).
18. Y. Liu, Z. G. Liu, S. M. Chen, M. Han, and W. Peng, "Microcapillary-based high-sensitivity and wavelength-tunable optical temperature sensor," IEEE Photon. Technol. Lett. **27**, 447–450 (2015).
19. Y. Liu, S. M. Chen, Q. Liu, and W. Peng, "Micro-capillary-based evanescent field biosensor for sensitive, label-free DNA detection," Opt. Express **23**, 20686–20695 (2015).
20. S. M. Chen, Y. Liu, Q. Liu, and W. Peng, "Temperature-compensating fiber-optic surface plasmon resonance biosensor," IEEE Photon. Technol. Lett. **28**, 213–216 (2016).
21. A. D. Kersey, M. A. Davis, H. J. Partrick, M. LeBlanc, K. P. Koo, C. G. Askins, M. A. Putnam, and E. J. Friebele, "Fiber grating sensors," J. Lightwave Technol. **15**, 1442–1463 (1997).